

Article

Tele-Operated Bilateral Control of Hydraulic Manipulator Using a Robust Controller Based on the Sensorless Estimated Reaction Force

Karam Dad Kallu, Saad Jamshed Abbasi, Hamza Khan, Jie Wang  and Min Cheol Lee *

School of Mechanical Engineering, Pusan National University, Busandaehak-ro 63 beon-gil, Jangjeon-dong Geumjeong-gu, Busan 46241, Korea; karamdadkallu@gmail.com (K.D.K.); saadjamshed93@gmail.com (S.J.A.); hamzakhan.0496@gmail.com (H.K.); wj@pusan.ac.kr (J.W.)

* Correspondence: mclee@pusan.ac.kr; Tel.: +82-10-3861-2688

Received: 29 March 2019; Accepted: 9 May 2019; Published: 15 May 2019



Featured Application: Applicable for higher order degree of freedom (DOF) manipulator used for dismantling in nuclear power plant (NPP).

Abstract: In nuclear power plants (NPP), dismantling is the most technically involved process during their life time. During the dismantling process, public safety must be ensured. In crisis situations, a remotely controlled robot system is needed for the dismantling of NPP. Therefore, in this research, a bilateral tele-operation system is proposed to tackle these emergency conditions. Transparency can be improved by using force and position signal in the control strategy. In some applications, force cannot be determine directly using physical sensors. In this work, a novel tele-operated bilateral control strategy is proposed to estimate the reaction force of 3-degree-of-freedom (DOF) master and hydraulic slave manipulators without the use of a sensor. The control strategy is developed by using sliding mode control with sliding perturbation observer (SMCSPO). The sliding perturbation observer (SPO) estimates the reaction force at the end effector and second link without using sensors. The sliding mode control (SMC) is used as a tele-operated bilateral controller for the robust position tracking and control of the slave device. The impedance model is used to differentiate between the applied force (force exerted by operator) and the reaction force due to the remote environment. Different experiments were performed to verify the proposed strategy. The results indicate that the slave manipulator exactly follows the trajectory of the master device. A camera is used to take visual feedback of the workspace for safety purpose. This technique can also be applied for higher-order DOF manipulators in NPP.

Keywords: SMCSPO; hydraulic manipulator; tele-operation; bilateral control; master-slave; estimated reaction force; position tracking; visual feedback

1. Introduction

The dismantling of a nuclear power plant (NPP) at the end of its life is an important issue. Among 160 NPP, nineteen of them have already been dismantled, and around one hundred are still under the process of dismantling [1–3]. The dismantling process has many stages. Among these, the complete dismantling of the structure and technical equipment, the gathering and storing of waste products, and the transportation of these items and the disposal of radioactive material in a controlled and safe environment are the most important. Automative/Tele-operated equipment/robot systems can play an important role in such scenarios. Past statistics show that several dismantling facilities based on robotic systems have worked well [4]. Thus, research is required to improve this technology in order to carry out the dismantling process efficiently.

The remote handling of a system/plant can be divided into several subcategories depending upon the application. For example, cutting requirements/equipment, segmentation, de-contamination of area/building, sampling, and utilization of remote systems [5–12]. France has developed a robotic system to dismantle nuclear power plants called the Maestro-robot-system [13,14]. Some researchers have proposed the use of tele-operated systems for performing such activities. Tele-operated systems in nuclear environments provide the operator only with visual feedback in order to get a sense of the reality of the working environment by using existing technologies. In tele-operated tasks, a controller is designed for a patched-up master and slave system. It controls the information flow accordingly. This methodology is also known as bilateral control activity. Several research groups have previously published articles on bilateral control strategies [15–18]. Two-channel architectures in bilateral control are the most popular. Force/force (F-F), position/position (P-P), position/force (P-F) and force/position (F-P) architecture designs are all two-channel architectures. Several other studies have also presented 3- or 4-channel architecture design for such activities [15–18]. Some of them have also discussed recent advancements in architectural design, controller performance, etc. [19,20]. Farooq et al. [21] proposed a design for a bilateral controller for application in non-linear tele-operated systems.

In [22], the authors presented an idea for a finite time problem for bilateral control strategies. A tele-operated system was considered in this study, and an output-feedback approach was implemented. Su et al. [23] proposed an adaptive back stepping control strategy for the slave system, whereas the master system was controlled by designing a robust controller. KD et al. [24] utilized a sliding mode control scheme with sliding perturbation observer (SMCSPO) to determine the reaction force for a three-link robotic manipulator. An interesting design for a joystick controller for bilateral tele-operated tasks was presented by Truong et al. [25]. The authors studied the results for application in construction machinery. The control strategy was based upon force-reflective gain in a master/slave system. A similar study for bilateral tele-operated tasks using underactuated mechanical systems was presented by Mejia et al. [26]. Mellah et al. [27] proposed the idea of utilizing adaptive neural fuzzy controllers with additional compensatory fuzzy control for a master/slave system. A force-position scheme was chosen, with an architecture based upon a two-channel bilateral tele-operative task. This strategy incorporates the localization of the slave device and the force reflection of master device. Xu et al. [28] discussed stability and transparency in the case of communication delays. They implemented a model-mediated tele-operative scheme.

Liu et al. [29] presented a unique and novel idea whereby the remote controller was not co-located with the manipulator device. The authors further analyzed stability and transparency. They discussed two difficult cases: one for fixed time delays, and the other for variable time delays. For the first case, a PD-like controller was chosen, while for the second case, a P-like controller was adopted. Abut et al. [30] presented a study involving a bilateral tele-operative task for a master/slave device and one virtual device. The localization and velocity control were proposed for the tele-operative task, with a specially designed visual interface for ease of use. The stability of the design was analyzed using the conventional Lyapunov strategy. Islam et al. [31] discussed the shared-tele-operative robotic system with un-symmetric variable delays. They implemented a robust control scheme based on state and impedance reflection. Additionally, they proposed an adaptive approach for determining interaction properties between the operator and the master device, and between the slave system and the real environment. Subsequently, the estimated delayed interaction properties were reflected back to the master/slave systems to overlap with the estimated impedance interactions properties between operator and environment. Sun et al. [32] presented a novel scheme for improving control of tele-operated devices by implementing prescribed performance controls and a wave-based time-domain passivity methodology. The extended prescribed performance control ensures synchronization of velocity, force and position. A standard Lyapunov approach was discussed for studying stability and performance. The results showed that the proposed control not only accurately tracked the velocity, position and force profiles, but also controlled the system's passivity. Azimifar et al. [33] discussed the estimation of the external forces acting on the master/slave devices. The main advantage of this

scheme is the elimination of the force sensor signal. This results in low cost for practical applications. The stability of the proposed scheme was also discussed using the conventional Lyapunov scheme.

The feedback signal based on touch is at the heart of bilateral tele-operative tasks. The master manipulator is operated by human being who depends on the actuator's signal, whereas the slave manipulator is installed in a remote environment and run through the hydraulic actuator's signal. Sakaino et al. [34] proposed the idea of utilizing a combination of different techniques to attain the best tracking control and stable results. They proposed the use of oblique-coordinate control to de-couple the force and position controllers. Furthermore, they linearized the hydraulic actuator's signal. Soltani et al. [35] proposed the hybrid-force and position control schemes for applying a fixed force to heart tissue with synchronization along the desired trajectory. Input-constrained predictive tracking control was presented utilizing a non-linear model. The performance results show that the catheter generated a force with root-mean-square-estimation (RMSE) of 4.9 mm and localization tracking with RMSE of 0.89 mm. Wang et al. [36] discussed the trajectory control for underwater manipulator systems by applying a discrete time-delay estimation methodology. Liu et al. [37] investigated the adaptive control law to achieve accurate tracking of the desired position. They also considered the uncertainties and non-linearities, as well as the dead-zones. Their proposed algorithm robustly estimated manipulator dynamics based on non-linear parameters, which were later fed into the controller. Their results provide evidence for the fact that the proposed controller scheme performs well, even when dynamic and dead-zone uncertainties appear simultaneously. Several studies in the field of bilateral control have investigated force sensors for determining external force. However, it has been shown in the literature that in radioactive dismantling tasks, these sensors have major drawbacks. A manipulator system equipped with force sensors performs as a 2 mass resonator. This reduces the sense of high frequency force [38]. A manipulator device consisting of a master/slave configuration is very attractive for application in the nuclear power plant dismantling process, as operator access is limited due to the possible radiation and the high load of material handling that is involved. However, it is difficult to use force sensors to realize force feedback in highly radioactive environments, because the force sensor will break as time passes.

This paper implements tele-operated bilateral control of a hydraulic manipulator using sliding mode control with sliding perturbation observer (SMCSPO) for sensor-less force feedback. It is an efficient and robust control algorithm that not only estimates the reaction force of the master and the slave, but also applies this estimated reaction force to the tele-operated bilateral control of the hydraulic manipulator of a 3 degree of freedom (DOF) master/slave robot. The reason for using a hydraulic manipulator is that its power-to-weight ratio is better than any other type of actuated robot at the expense of positional accuracy. In this research, the sliding perturbation observer (SPO) is implemented to estimate the reaction force of the slave without using any sensor. The tele-operated bilateral control scheme is implemented for efficient and accurate position and force tracking betweenin the master/slave configuration with visual feedback. In the bilateral controller, the difference of the reaction force of the slave manipulator and the operating force applied to the master manipulator is designed to target the impedance model. The reaction force of the slave is a result of the effects in the remote environment, while the operator force is applied by the operator (human) at the master manipulator. The experimental results of our studies confirm that the slave efficiently follows the position trajectory of the master system.

The remainder of the manuscript is structured as follows: Modeling and dynamics of the hydraulic manipulator are described in Section 2; the theory of sliding mode control with sliding perturbation observer and the algorithm for estimating reaction force are presented in Section 3; the tele-operated bilateral-control strategy is described in Section 4; the details of the experimental setup are summarized in Section 5; the results are shown in Section 6; and concluding remarks regarding the study are provided in Section 7.

2. Modeling and Dynamics of the Hydraulic Manipulator

Several applications in the machine tool/handling industry have utilized hydraulic systems in past. These applications include the handling of hazardous material, heavy industry, oil and gas exploration, etc. Servo systems can be designed to estimate different parameters, such as acceleration, force, temperature profile, and voltage/current, among others. The advantageous features of hydraulic actuators include robust response, broad range and limited stroke, etc., in addition to zero backlash, less wear and tear, and accurate control. Generic schematic diagrams of a 3-DOF hydraulic manipulator utilized for dismantling nuclear power plants are shown in Figures 1 and 2. Hydraulic systems used for dismantling nuclear power plants include a couple of hydraulic cylinders for the two links and an AC servo-motor for the base. The dismantling process requires a greater force to produce vertical moment as compared to the force required to produce horizontal moment. The hydraulic manipulator is modeled using the signal compression method [39].

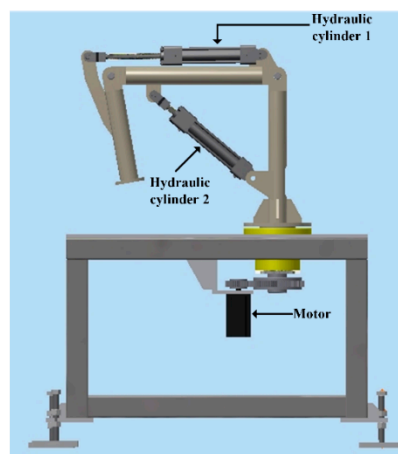


Figure 1. Schematic diagram of the hydraulic manipulator.

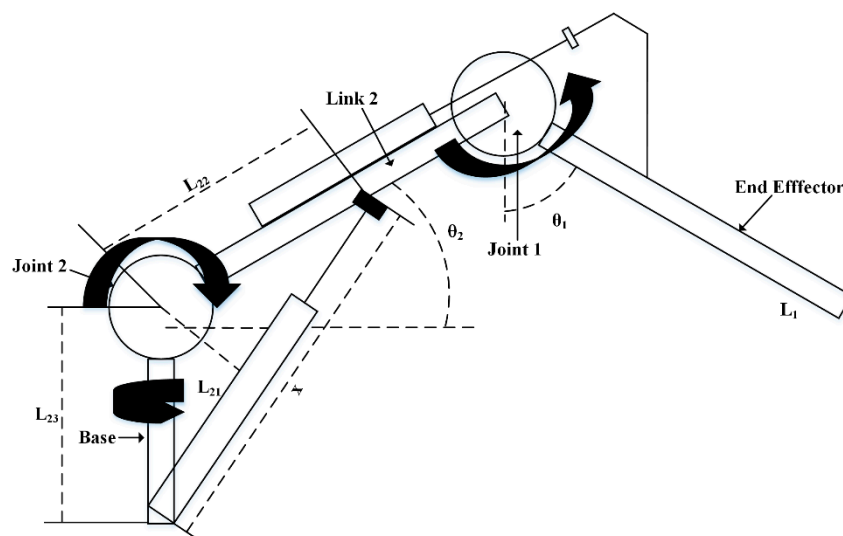


Figure 2. Schematic diagram of the base, 2nd link and end effector.

The modeling equations of a manipulator depend upon localization, different forces, and acceleration properties, which can be mathematically written as,

$$T = A(\theta)\ddot{\theta} + B(\theta, \dot{\theta}) + g(\theta) \tag{1}$$

where θ = angle of joints, $A(\theta)$ = mass/inertia matrix, $B(\theta, \dot{\theta})$ = centrifugal/coriolis torque, $g(\theta)$ = joint space gravity torque and T = vector of joint torques. Equations for different dynamical properties of links can be written as:

$$(J_{s1} + \Delta J_{s1})\ddot{\theta}_1 + (D_{s1} + \Delta D_{s1} + \beta_1)\dot{\theta}_1 + 0.5M_{s1}L_1g \sin \theta_1 + \tau_{e1} = T_1 \tag{2}$$

$$(J_{s2} + \Delta J_{s2})\ddot{\theta}_2 + (D_{s2} + \Delta D_{s2})\dot{\theta}_2 + M_{s2}L_{2cm}g \cos \theta_2 + \beta_2\dot{x} + \tau_{e2} + \lambda = T_2 \tag{3}$$

$$(J_{s3} + \Delta J_{s3})\ddot{\theta}_3 + (D_{s3} + \Delta D_{s3})\dot{\theta}_3 + 0.5M_{s3}L_3g \sin \theta_3 + \tau_{e3} = T_3 \tag{4}$$

where J_{s1} J_{s2} J_{s3} , D_{s1} D_{s2} D_{s3} , M_{s1} M_{s2} M_{s3} , and T_1 T_2 T_3 denote the inertia, damping, mass and torques of the base, 2nd link, and end effector, respectively. Δ denotes the uncertainty term, and β_1 and β_2 represent the viscosity of the cylinders. L_1 and L_3 are the lengths of the base and the end effector, L_2 represents the length from the joint to the center of mass (COM) of the 2nd link. λ in Equation (3) denotes a dynamic torque effect at joint 2 by hydraulic cylinder motion attached to link 2 to rotate the end effector of the manipulator, $\dot{\theta}_1$ and \dot{x} are the velocities of the 1st and 2nd cylinders, respectively. τ_{e1} , τ_{e2} and τ_{e3} denote the reaction torque generated by contact with the environment and joints 1, 2 and 3, respectively.

3. Sliding Mode Control with Sliding Perturbation Observer (SMCSPO)

SPO and SMC has shown efficient performance against perturbation in many studies by employing partial state feedback. The combination of SMC and SPO is known as sliding mode control with sliding perturbation observer (SMCSPO) [40]. In this work, SMC and SPO are used respectively to control and to estimate the reaction force of a 3DOF robotic manipulator. Generally, second-order dynamics of n-DOF can be represented as

$$\ddot{x}_j = f_j(x) + \Delta f_j(x) + \sum_{i=1}^n [(b_{ji}(x) + \Delta b_{ji}(x))u_i] + d_j(t) \tag{5}$$

where $x \triangleq [x_1 \dots x_n]^T$ denotes the state vector, $f_j(x)$ and $\Delta f_j(x)$ are the non-linear driving force and uncertainties, respectively, b_{ji} is the control gain matrix with corresponding uncertainties Δb_{ji} , d_j is the external disturbance, and u_j is the control input. f_j , b_{ji} are well-known continuous functions of state, described in [41]. All these uncertainties in joint form can be defined as perturbation, with the mathematical form of the perturbation being as follows,

$$\psi_j(x, t) = \Delta f_j(x) + \sum_{i=1}^n [\Delta b_{ji}(x)u_i] + d_j(t) \tag{6}$$

It is assumed that the perturbations are upper bounded by a known continuous function of the state. The continuous function of the state for the upper bound of the perturbation can be defined as follows:

$$\Gamma_j(x, t) = F_j(x) + \sum_{i=1}^n |\Phi_{ji}(x)u_i| + D_j(t) > |\Psi_j(t)| \tag{7}$$

where $F_j > |\Delta f_j|$, $\Phi_{ji} > |\Delta b_{ji}|$ and $D_j > |d_j|$ represent the expected upper bounds of the uncertainties. Let us suppose $f_j(x)$, defined in Equation (5), except the perturbation of Equation (6) is represented as

$$f_j(\hat{x}) + \sum_{i=1}^n b_{ji}(\hat{x})u_i = \alpha_{3j}\bar{u}_j \tag{8}$$

where $\alpha_{3j} > 0$, and \bar{u}_j is a new control variable. The SPO equations are derived as in [40].

$$\dot{\hat{x}}_{1j} = \hat{x}_{2j} - k_{1j} \text{sat}(\bar{x}_{1j}) \tag{9}$$

$$\dot{\hat{x}}_{2j} = \alpha_{3j} \bar{u}_j - k_{2j} \text{sat}(\bar{x}_{1j}) + \hat{\Psi}_j \tag{10}$$

$$\dot{\hat{x}}_{3j} = \alpha_{3j}^2 (\bar{u}_j + \alpha_{3j} \hat{x}_{2j} - \hat{x}_{3j}) \tag{11}$$

$$\dot{\hat{\psi}}_j = \alpha_{3j} (\alpha_{3j} \hat{x}_{2j} - \hat{x}_{3j}) \tag{12}$$

where $k_{1j}, k_{2j}, \alpha_{3j}$ are greater than zero and $\bar{x} = \hat{x} - x$ is the estimation error. $\hat{\psi}_j =$ estimated perturbation.

$$\text{sat}(\bar{x}_{1j}) = \begin{cases} \bar{x}_{1j}/|\bar{x}_{1j}|, & \text{if } |\bar{x}_{1j}| \geq \varepsilon_{0j} \\ \bar{x}_{1j}/\varepsilon_{0j}, & \text{if } |\bar{x}_{1j}| \leq \varepsilon_{0j} \end{cases} \tag{13}$$

The sliding function is defined as follows:

$$s_j = \dot{e}_j + c_{1j} e_j \tag{14}$$

where $e_j = x_{1j} - x_{1jd}$ is the actual position tracking error, $c_{1j} > 0$. As the sliding surface is reached, we define $\dot{s}_j = 0$, and the sliding control is represented as

$$\dot{s}_j = -K_j \text{sat}(s_j) \tag{15}$$

The new control input \bar{u}_j is designed such that it forces $\dot{\hat{s}}_j < 0$ outside of the prescribed manifold. The desired \hat{s}_j dynamics is represented as

$$\dot{\hat{s}}_j = -K_j \text{sat}(\hat{s}_j) \tag{16}$$

Thus, $\dot{\hat{s}}_j$ can be calculated as

$$\dot{\hat{s}}_j = \alpha_{3j} \bar{u}_j - \left[k_{2j}/\varepsilon_{0j} + c_{j1} (k_{1j}/\varepsilon_{0j}) - (k_{1j}/\varepsilon_{0j})^2 \right] \bar{x}_{1j} - (k_{1j}/\varepsilon_{0j}) \bar{x}_{2j} - \ddot{x}_{1jd} + c_{j1} (\hat{x}_{2j} - \dot{x}_{1jd}) + \hat{\psi}_j \tag{17}$$

The control law is defined as

$$\bar{u}_j = \frac{1}{\alpha_{3j}} \left\{ -K_j \text{sat}(\hat{s}_j) + \left[\frac{k_{2j}}{\varepsilon_{0j}} + c_{j1} \frac{k_{1j}}{\varepsilon_{0j}} - \left(\frac{k_{1j}}{\varepsilon_{0j}} \right)^2 \right] \bar{x}_{1j} + \ddot{x}_{1jd} - c_{j1} (\hat{x}_{2j} - \dot{x}_{1jd}) - \hat{\psi}_j \right\} \tag{18}$$

In the above equation, \bar{u}_j is a control input of SMCSPO. The actual s_j dynamics within the boundary layer $|\hat{s}_j| \leq \varepsilon_{0j}$ becomes

$$\dot{s}_j + \frac{K_j}{\varepsilon_{0j}} s_j = \left[\frac{k_{2j}}{\varepsilon_{0j}} - \left(\frac{k_{1j}}{\varepsilon_{0j}} - \frac{K_j}{\varepsilon_{0j}} \right) \left(c_{j1} - \frac{k_{1j}}{\varepsilon_{0j}} \right) \right] \bar{x}_{1j} - \left(c_{j1} + \frac{K_j}{\varepsilon_{0j}} \right) \bar{x}_{2j} - \ddot{\psi}_j \tag{19}$$

The designed controller (SMCSPO) reduces the error between the real and the desired trajectories. The mechanical hardware limitations restrict the design procedure as described in Jairo et al. [40].

The instant at which $|\hat{s}_j| \leq \varepsilon_{0j}$, the observer design, and the s_j dynamics can be represented in mathematical form as shown below:

$$\begin{bmatrix} \dot{\tilde{x}}_{1j} \\ \dot{\tilde{x}}_{2j} \\ \dot{\tilde{x}}_{3j} \\ \dot{s}_j \end{bmatrix} = \begin{bmatrix} -k_{1j}/\varepsilon_{0j} & 1 & 0 & 0 \\ -\frac{k_{2j}}{\varepsilon_{0j}} & \alpha^2_{3j} & -\alpha_{3j} & 0 \\ 0 & \alpha^3_{3j} & -\alpha^2_{3j} & 0 \\ k_{2j}/\varepsilon_{0j} - (c - k_{1j}/\varepsilon_{0j})^2 & -(2c + \alpha^2_{3j}) & \alpha_{3j} & -c \end{bmatrix} \begin{bmatrix} \tilde{x}_{1j} \\ \tilde{x}_{2j} \\ \tilde{x}_{3j} \\ s_j \end{bmatrix} + \begin{bmatrix} 0 \\ 0 \\ 1 \\ 0 \end{bmatrix} \dot{\psi}_j/\alpha_{3j} \quad (20)$$

where a square matrix of order 4 in Equation (20) represents the state matrix. Further supposing that λ represents the eigenvalues of the state matrix A , then its characteristic equation $\det|\lambda I - A| = 0$ can be expressed as,

$$[\lambda + c_{j1}][\lambda^3 + (k_{1j}/\varepsilon_{0j})\lambda^2 + (k_{2j}/\varepsilon_{0j})\lambda + \alpha^2_{3j}(k_{2j}/\varepsilon_{0j})] = 0 \quad (21)$$

By implementing the pole-placement method, let us introduce a desired characteristic polynomial $p(\lambda_d) = (\lambda + \lambda_d)^4$ which leads to a design solution

$$k_{1j}/\varepsilon_{0j} = 3\lambda_d k_{2j}/k_{1j} = \lambda_d \alpha_{3j} = \sqrt{\lambda_d/3c} = K_j/\varepsilon_{0j} = \lambda_d \quad (22)$$

It is clear from the equation that higher values of gain λ_d guarantee higher accuracy. In [41], the authors showed the limitations of sliding function dynamics. They suggested that λ_d should be less than $1/5\tau^{hw}$, where w is the frequency and h is a positive number. These results were also validated in another study [42]. In this work, we selected the value of optical gain by using following formula:

$$\lambda_d = \frac{1}{15\tau^{hw}} \quad (23)$$

Estimation of Reaction Force Using Sliding Perturbation Observer (SPO)

The SPO can be used to estimate the perturbation, leading to the determination of the reaction forces. The estimation of perturbations consists of two factors: the external disturbance, and the dynamic error due to nonlinearities of gravity and friction. Equations (2) and (3) can be used to estimate the perturbation.

$$\hat{\psi}_{s1} = -\frac{1}{J_{s1}}(\hat{\tau}_{e1}) - \frac{1}{J_{s1}}(0.5M_{s1}L_1g \sin \theta_1) - (\frac{\Delta J_{s1}}{J_{s1}})\ddot{\theta}_1 - \frac{1}{J_{s1}}(\Delta B_{s1} + \beta_1)\dot{\theta}_1 \quad (24)$$

$$\hat{\psi}_{s2} = -\frac{1}{J_{s2}}(\hat{\tau}_{e2}) - \frac{1}{J_{s2}}(M_{s2}L_2g \cos \theta_2) - (\frac{\Delta J_{s2}}{J_{s2}})\ddot{\theta}_1 - \frac{1}{J_{s2}}(\Delta B_{s2}\dot{\theta}_2) - \frac{1}{J_{s2}}(\beta_2\dot{x}) - \frac{1}{J_{s2}}(\lambda) \quad (25)$$

Equations (24) and (25) can be rewritten as

$$\hat{\tau}_{e1} = J_{s1}\hat{\psi}_{s1} + 0.5M_{s1}L_1g \sin \theta_1 + \Delta J_{s1}\ddot{\theta}_1 + (\Delta B_{s1} + \beta_1)\dot{\theta}_1 \quad (26)$$

$$\hat{\tau}_{e2} = J_{s2}\hat{\psi}_{s2} + M_{s2}L_2g \cos \theta_2 + \Delta J_{s2}\ddot{\theta}_1 + \Delta B_{s2}\dot{\theta}_2 + \beta_2\dot{x} + \lambda \quad (27)$$

where $\hat{\tau}_{e1}$ and $\hat{\tau}_{e2}$ are the estimated reaction torques of the end effector and the 2nd link, respectively. It is worth mentioning that if the parameter is well estimated, then the parameter of uncertainty could be considered as well.

4. Tele-Operated Bilateral Control for 3DOF Hydraulic Manipulator

4.1. Tele-Operated Bilateral Control

The client and server systems are turned ON. The client, in this case, is the slave, and the server is the master robotic system. The essential safety procedures are followed to ensure that no harm can be done to the environment due to leakage of hydraulic fluids or electric wires. The application of the slave robotic system is carried out after the execution of the master side. Both applications are Windows-based desktop applications developed using Microsoft Visual Studio. The slave robotic system has the parameters required for a server to send a connection request. The master robotic system remains in the listening state, waiting for incoming connections through the network interface on the known IP and port number. When the master robotic system receives an incoming connection request, it verifies the legitimacy of the client. The client completes the verification request by providing the requested parameters; only then does the server establish a communication channel. The application displays the connection status and shows a notification when the connection has been successfully established. The amplifiers are turned OFF, and after a small delay, they are turned back ON by the master and slave applications when connection has been established. The application includes buttons for turning the amplifiers OFF and ON. Operation starts from the master side, and this is subsequently followed by the master upon pressing the Read button on both sides. The master application acquires the data from encoders attached to the axes of the robotic system and computes the desired parameters according to the system equations. These parameters are vital for our tele-operated robotic system. The computed parameters, along with the orientation of axes, are then disseminated to client side. The network sockets are used to transfer information between the master and the slave robotic systems. The slave/client application receives the information from the master through its socket. The slave robotic system is then actuated by the application according to the parameters provided by the master. The slave application also computes the reaction force while moving similarly to the master robotic system. The computation is performed using the SMCSP0 algorithm. The slave application measures the position and estimates the perturbation. This information is sent back to the master robotic system. This flow of information continues, and the system has been tested over short and long durations. The slave robotic system keeps tracking the master robotic system. The system flow diagram is shown in Figure 3. If either side (master or slave) stops the application or the network is disconnected, the other side receives a notification of connection closure. The connection-related notifications are shown, along with the application environment, in Figure 4.

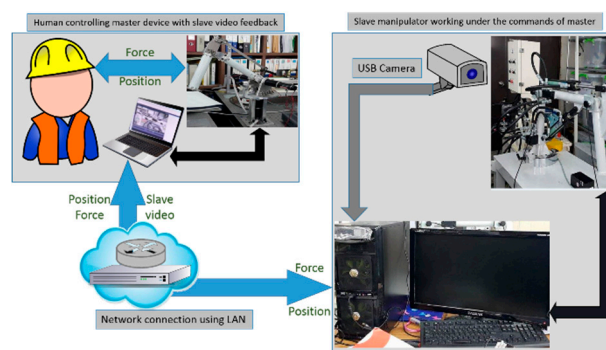


Figure 3. Schematic diagram of tele-operation.

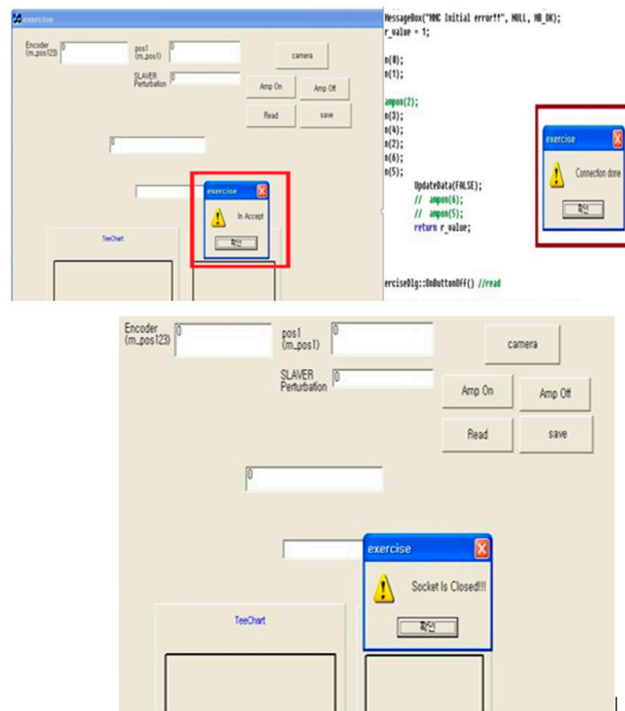


Figure 4. Client server (master and slave) connection confirmation status.

4.2. Bilateral Control

The bilateral control is designed to provide a realistic feel for the operator at the master device that corresponds to the environment at the slave device. In other words, there are two significant factors that need to be addressed. The 1st one is that the slave system tracks the commands from the master device, and other is that the operator himself feels like part of environment at the slave device, with a real feeling of reaction force. The master/slave system’s dynamical equations are

$$J_m \ddot{\theta}_m + B_m \dot{\theta}_m = u_m + \tau_h \tag{28}$$

$$J_s \ddot{\theta}_s + B_s \dot{\theta}_s = u_s - \tau_e \tag{29}$$

where J and u represent inertia and control input with subscript m and s representing the master and slave systems, respectively. Real/action generated by the operator at the master device and reaction force of the slave system in a remote environment are represented by τ_h and τ_e . The schematic of the designed bilateral control is presented in Figure 5.

The operator at the master device commands/controls its movement, which is followed by the slave device. The SMC defines the logic behind the movement of the slave device. As the slave device follows the movement of the master device, the impedance controller is responsible for finding the reaction force accordingly. If the connection betweenbetween the slave device and and environment is null, the operator does not fell any reaction force.

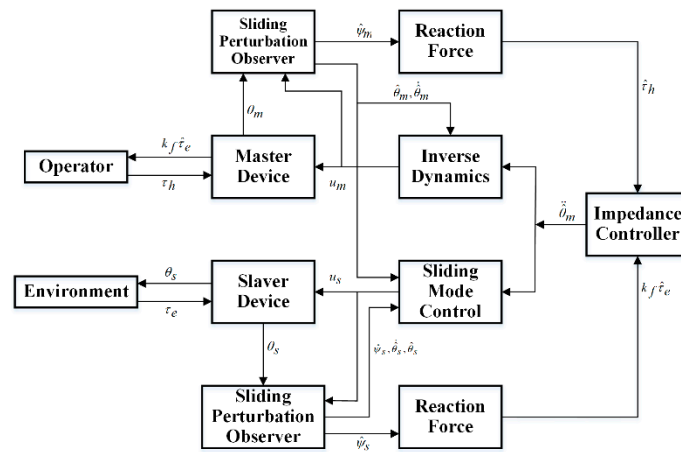


Figure 5. Structure of bilateral control.

4.3. Master Controller and Device

The master device was planned by considering two important features. The 1st is that the reaction force must be perceived by humans when the slave device makes contact with the environment. The 2nd is that relatively less force should be required by the operator to operate the master device. The impedance control in the master device incorporates these two factors, which can be mathematically represented as follows:

$$J_d \ddot{\theta}_m + B_d \dot{\theta}_m + K_d \theta_m = \hat{\tau}_h - k_f \hat{\tau}_e \tag{30}$$

where J_d , B_d and K_d represent parameters in impedance control defining inertia, damping and stiffness, respectively; $k_f = 1$ is used to scale the reaction force; k_f defines the force ratio transmitted by the master device to the slave manipulator. The control input for the master device is calculated by using observed states, i.e., Equations (28) and (30), as follows:

$$u_m = (B_m - \frac{J_m}{J_d} B_d) \dot{\theta}_m + (\frac{J_m}{J_d} - 1) \hat{\tau}_h - \frac{J_m}{J_d} (k_f \hat{\tau}_e + K \hat{\theta}_m) \tag{31}$$

where u_m , $\dot{\theta}_m$ and $\hat{\theta}_m$ are the control input, estimated speed profile, and estimated position profile for master device, respectively; $\hat{\tau}_h$ is the estimated torque for the operator. The master manipulator considered in this study is shown in Figure 6.

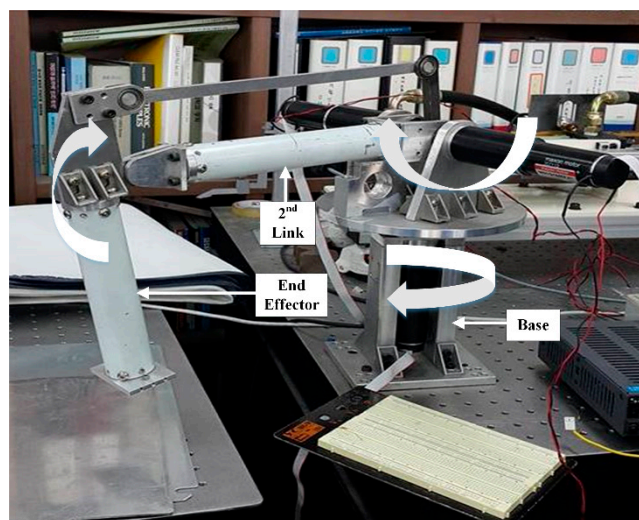


Figure 6. Master device.

4.4. Slave Controller and Device

The master device gives commands to the slave device, which follows them. The controller for the slave device is designed based on the SMCSPO scheme. The estimated perturbation obtained using the SMCSPO scheme includes only the computation of uncertainties, non-linearities and disturbances. The beauty of SMCSPO is that it guarantees overcoming the problematic situations of non-linearities, uncertainties in parameter values, and disturbances in the design system. The estimated sliding function is derived as

$$\hat{s} = \dot{\hat{e}} + c\hat{e} \tag{32}$$

where tracking error is defined as $\hat{e} = \hat{\theta}_{s1} - \hat{\theta}_{m1}$, c is greater than zero. By putting the observed/estimated state into the sliding function defined above in Equation (32) and the sliding perturbation observer of Equation (12), the differential of the estimated sliding surface \hat{s} can be mathematically denoted as

$$\dot{\hat{s}} = \alpha_{s3}\bar{u}_s - \frac{k_{s2}}{\varepsilon_{s0}}\tilde{\theta}_{s1} - \alpha_{s2}\tilde{\theta}_{s1} + \hat{\psi}_s - \frac{k_{s1}}{\varepsilon_{s0}}\tilde{\theta}_{s1} - \alpha_{s1}\tilde{\theta}_{s1} - \ddot{\theta}_{m1} + c(\dot{\theta}_{s1} - \dot{\theta}_{m1}) \tag{33}$$

It is found that $\alpha_{s1}, \alpha_{s2} \approx 0$ when the phase is converged to the sliding surface, and the error estimate $\tilde{\theta}_{s1}$ remains inside the boundary layer. The impedance model in Equations (30) and (33) are utilized to obtain $\dot{\hat{s}}$

$$\dot{\hat{s}} = \alpha_{s3}\bar{u}_s - \left[\frac{k_{s2}}{\varepsilon_{s0}} + c\left(\frac{k_{s1}}{\varepsilon_{s0}}\right) - \left(\frac{k_{s1}}{\varepsilon_{s0}}\right)^2 \right] \tilde{\theta}_{s1} - J_d^{-1}(\hat{\tau}_h - k_f\hat{\tau}_e - B_d\dot{\theta}_m - K_d\hat{\theta}_m) + \hat{\psi}_s + c(\dot{\theta}_{s1} - \dot{\theta}_{m1}) \tag{34}$$

The new control variable \bar{u}_s is chosen under this constraint, i.e., $\dot{\hat{s}} < 0$. Similarly, $\dot{\hat{s}}$ dynamics is chosen to satisfy the sliding mode condition.

$$\dot{\hat{s}} = -Ksat(\hat{s}) \tag{35}$$

The new control input presented in Equation (8) can be found from Equations (34) and (35)

$$\bar{u}_s = \alpha_{s3}^{-1} \{ -Ksat(\hat{s}) + \left[\frac{k_{s2}}{\varepsilon_{s0}} + c\left(\frac{k_{s1}}{\varepsilon_{s0}}\right) - \left(\frac{k_{s1}}{\varepsilon_{s0}}\right)^2 \right] \tilde{\theta}_{s1} + J_d^{-1}(B_d\dot{\theta}_m + K_d\hat{\theta}_m - \hat{\tau}_h + k_f\hat{\tau}_e) - c(\dot{\theta}_{s1} - \dot{\theta}_{m1}) - \hat{\psi}_s \} \tag{36}$$

Finally, the slave control input is defined as

$$u_s = J_s\bar{u}_s + B_s\dot{\theta}_s \tag{37}$$

5. Experimental Setup

Figure 7 shows the experimental setup of the slave device. The hydraulic manipulator has one servo motor and two cylinders. The hydraulic cylinder is used to actuate the 2nd link and the end effector, whereas the servo motor is used to control the base of the manipulator.

The 3DOF hydraulic manipulator was used to perform several experiments. The specifications of the hydraulic manipulator are listed in Table 1.

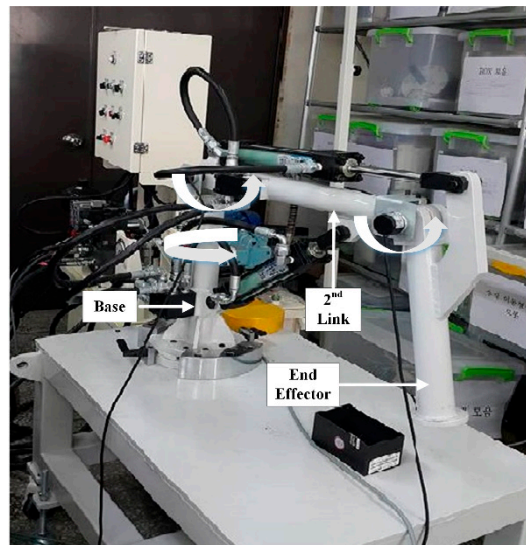


Figure 7. Slave device.

Table 1. Hydraulic manipulator specifications.

S. No	Items	Specification
1	Hydraulic cylinder	Stroke = 0.2 m Piston diameter = 0.04 m Rod diameter = 0.022m
2	Hydraulic pump	P_max = 210 bar Q_max = 20l/min
3	Displacement transducer	Stroke = 0.2 m (±10 V)
4	Control valve	D633-313A, Moog, Inc
5	Relief valve	P_set = 20 bar
6	Control board	PC-based MMC

D633-313A (Servo Tech Co., Korea).

Several previous studies have discussed identification schemes and control design strategies for hydraulic manipulators [43,44]. Such systems include a couple of hydraulic cylinders and an AC servo motor. Usually, signal compression methods are utilized to derive dynamical equations for all of the described systems. These methods provide an equivalent impulse signal and utilize correspondingly derived functions to estimate the dynamical model [45]. This dynamical model can be represented as

$$\ddot{x} = \frac{1}{J_i}u - \frac{1}{J_i}D_i\dot{x}, i = 1, 2, 3 \tag{38}$$

where D_i = damper and J_i = inertia. The values of the dynamics are presented in Table 2.

Table 2. Hydraulic manipulator dynamics parameters.

Links	Moment of Inertia (Master) $kg \cdot m^2$	Moment of Inertia (Slave) $kg \cdot m^2$	Damper (Master) $kg \cdot m^2/s$	Damper (Slave) $kg \cdot m^2/s$
1	1.35135	303.26	3.99	17,355.5
2	1.5	59.52	3.99	5241.66
3	0.74	355.91	3.99	2214

A pictorial view of the experimental setup is shown in Figure 8. It contains the master and slave systems and the corresponding control system.



Figure 8. Experimental setup.

The master/slave manipulators both have 3-links. The first link in both systems is mathematically connected to the base of the corresponding system. Reaction forces are generated at the end effector and the 2nd link. The reaction forces are calculated/estimated based on SMCSPO. The operator at the master manipulator generates commands for the master device that are subsequently followed by the slave device, and using a personal computer, the operator can take a visual look at the master device. The design of the SMC controls the trajectory of the slave device in accordance with the movement of the master device. The GUI for visual feedback is presented in Figure 9.



Figure 9. Video feedback.

6. Experimental Results

The SMCSPO parameter values used in the experiments are listed in Table 3.

Table 3. Design parameters.

Parameters	Value
K of base	8
K of 2 nd link	250
K of end effector	25
k_1	39
k_2	507
ϵ_0	1
c	13
e	1
α_3 (End Effector)	4.08
α_3 (2 nd Link)	10
α_3 (Base)	2.58

To verify the methodology, seven experiments were performed with SMCSPO under different scenarios. These experiments included: (i) tele-operated bilateral control of the end effector; (ii) estimation of the perturbation at the end effector of the master/slave; (iii) tele-operated bilateral control of the 2nd link; (iv) estimation of the perturbation at the 2nd link of the master/slave; (v) tele-operated bilateral control of the base; (vi) estimation of the perturbation at the base of the master/slave; and (vii) tele-operated bilateral control of the end effector and the 2nd link at the same time. The master and slave devices are shown in Figures 7 and 8. These experiments were performed in real-time scenarios in which the operator (human) set the master manipulator in movement, and the slave manipulator moved in accordance with this trajectory as evaluated by SMCSPO. The trajectory profiles for the end effectors of the master/slave devices are depicted in Figure 10. The trajectory for the master device’s end effector is presented as a red line, while for the slave device, it is shown as a blue line. It is evident that the slave’s end effector follows the master’s trajectory with only a very small degree of mismatch. It can also be seen that the trajectories of both of the end effectors attain a maximum value of 88.96 degrees at 18 s on the time scale. It is worth noting that the end effector of the slave has a workspace of 0–90 degrees.

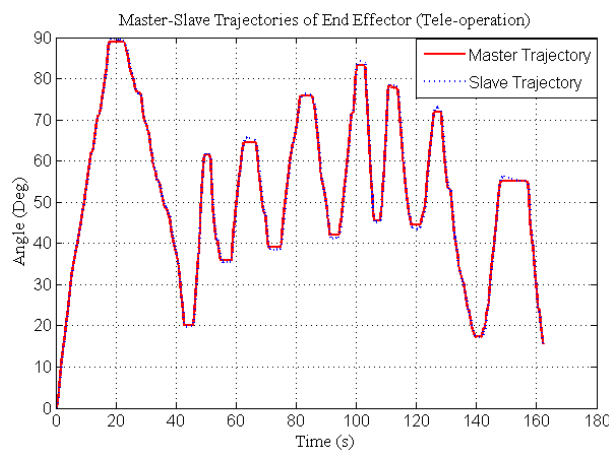


Figure 10. Master/slave trajectories for end effectors.

The relative errors of the trajectories of the end effectors of the master and slave manipulators are shown in Figure 11. It can be seen that maximum value of error between the master and slave trajectories was 0.94 degree at 157.71 s on the time scale. It is clear from Figure 11 that the error profile is very small, which shows the accuracy of the proposed method.

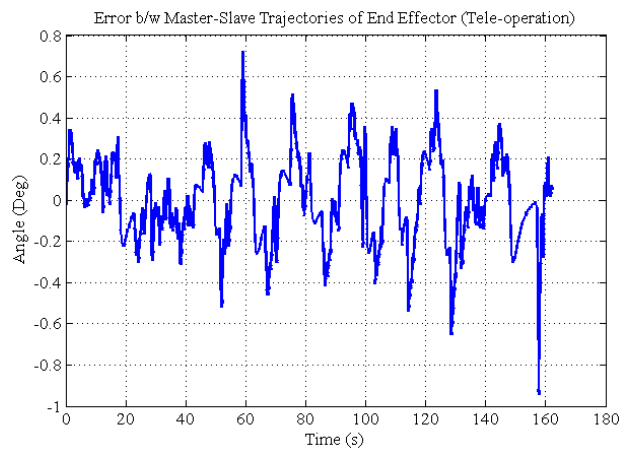


Figure 11. Error between the end effector trajectories for master and slave.

The estimated perturbations for the master’s and slave’s end effectors are presented in Figures 12 and 13, respectively. The maximum value of estimated perturbation for the master system was 90.87 N·m at 178.01 s, whereas for the slave system, this was 1635.72 N·m at 148.016 s.

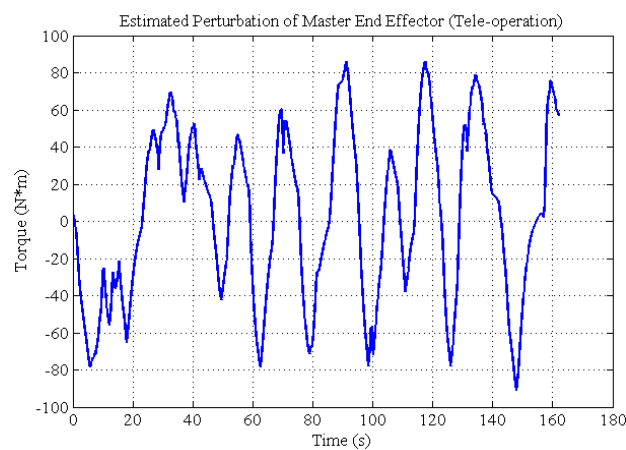


Figure 12. Estimated perturbation of the master end effector.

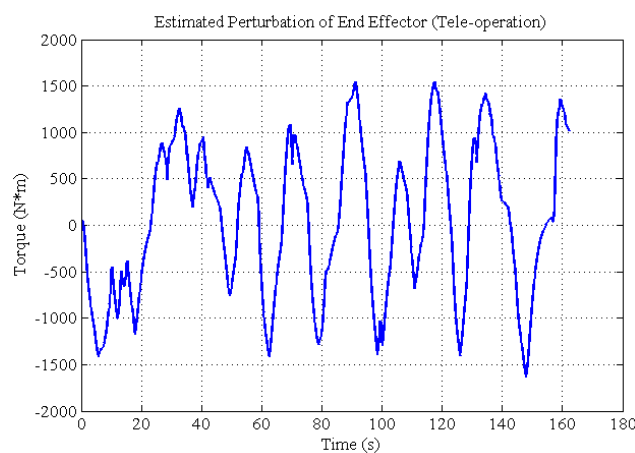


Figure 13. Estimated perturbation of the slave end effector.

It is evident from Figures 12 and 13 that the estimated perturbation corresponding to the slave system had a much higher value than that for the master device. The reason behind this is the hydraulic

system of the slave device. The dynamical value of the slave system is 303.26, which is higher than the value for the master device, which is 1.35135. The profiles for the estimated perturbations were similar, but with opposing directions. Numerically, the normalized values for estimated perturbation lay within the ranges [0, 1] and [−1, 0] for the master and slave systems, respectively. The normalized values were calculated as follows.

$$P_{norm}(Master) = \frac{a_i - \min(a)}{\max(a) - \min(a)}, i = 1 \dots N \tag{39}$$

$$P_{norm}(Slave) = \frac{a_i - \max(a)}{\max(a) - \min(a)}, i = 1 \dots N \tag{40}$$

where a_i is the i^{th} value of perturbation. The results for normalized estimated perturbation for the end effectors of both the master and slave systems are shown in Figure 14. The profile corresponding to the master device is shown as a red line, while that for the slave is shown as a blue line.

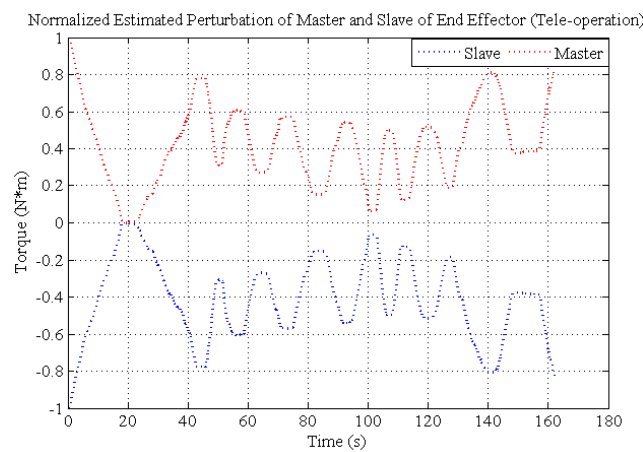


Figure 14. Normalized estimated perturbation of end effectors for master and slave.

The results for the 2nd link of the master device (blue line) and the slave device (red line) are presented in Figure 15. It is evident that slave’s 2nd link follows the master’s 2nd link effectively using SMCSP0. The space allows the 2nd link to move between 0 and 90 degrees. The maximum value of the profile is 60.13 degrees at 26.55 s on the time scale.

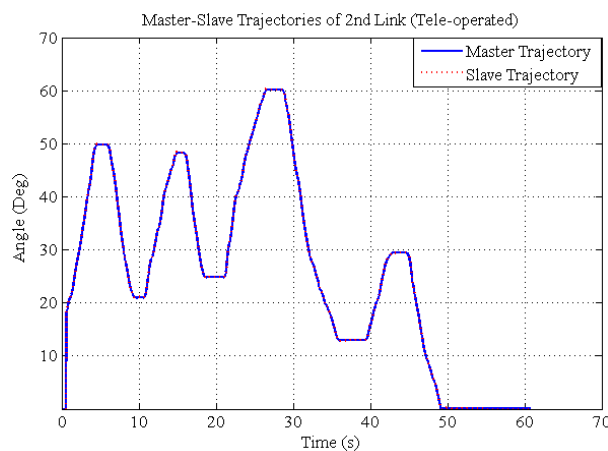


Figure 15. Master/slave trajectories for the 2nd link.

The mismatch profile for the trajectories of the 2nd link for the master and slave devices is shown in Figure 16. The maximum mismatch value for the corresponding trajectories was 0.55 degree at 21.68 s on the time scale.

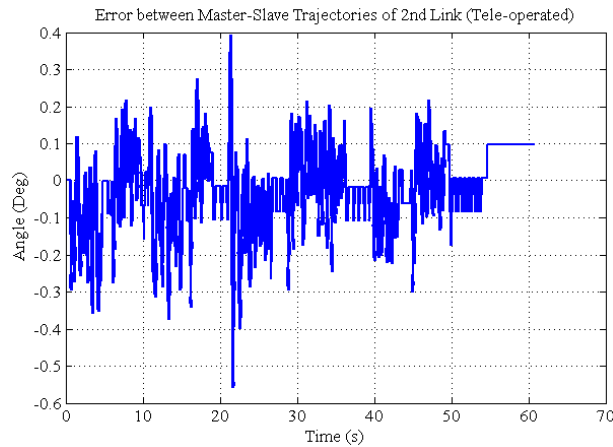


Figure 16. Error between master and slave trajectories for the 2nd link.

The estimated perturbations for the 2nd link of the master and the slave are presented in Figures 17 and 18, respectively. It can be seen that the maximum value of perturbation was 45.69 N·m at 21.47 s for the master’s 2nd link and 543.9 N·m at 21.47 s for the slave’s 2nd link. One important fact is that the estimated perturbation profiles are the same for both the master and slave devices, but in opposing directions.

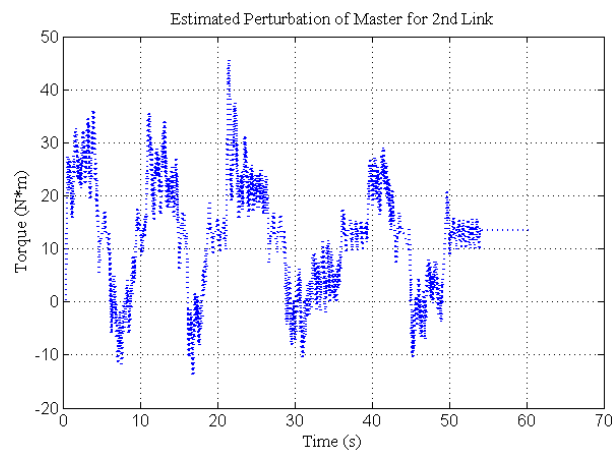


Figure 17. Estimated perturbation of the master’s 2nd link.

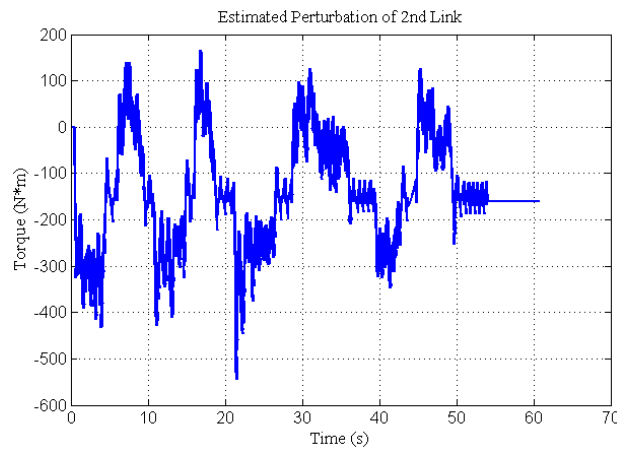


Figure 18. Estimated perturbation of the slave’s 2nd link.

The normalized estimated perturbations of the master device’s end link (red line) and the slave device’s 2nd link (blue line) are presented in Figure 19.

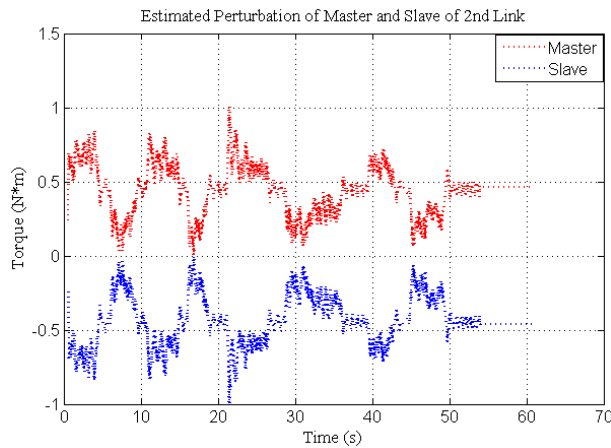


Figure 19. Normalized estimated perturbation of the 2nd link for the master and the slave.

The results of the experiments for the base trajectories of both the master and slave devices are shown in Figure 20. The base trajectory of the master device is shown as a red line, while that of the slave device is shown as a blue line. Accurate tracking of the slave shows the effectiveness of the proposed scheme. The available space for the base allows its movement between 0 and 360 degrees. The maximum value of the trajectory profile is 100.38 degrees at 23.2 s on the time scale.

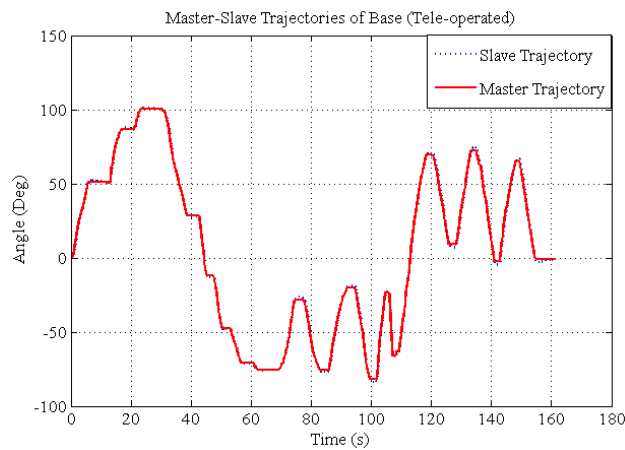


Figure 20. Master/slave trajectories for the base.

The mismatch in the tracking of the base is presented in Figure 21. The maximum mismatch was observed at 143.3 s on the time scale, with a value of 0.859 degrees.

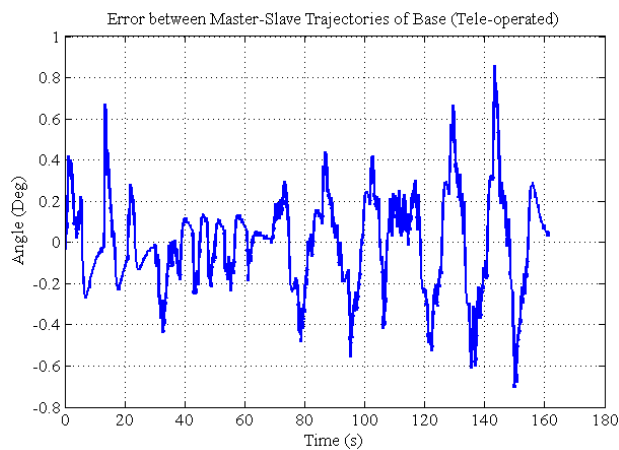


Figure 21. Error between the base trajectories for master and slave.

Figure 22 represents the estimated perturbation of the base. The maximum estimated perturbation of the master was 67.89 N·m at 140.96 s.

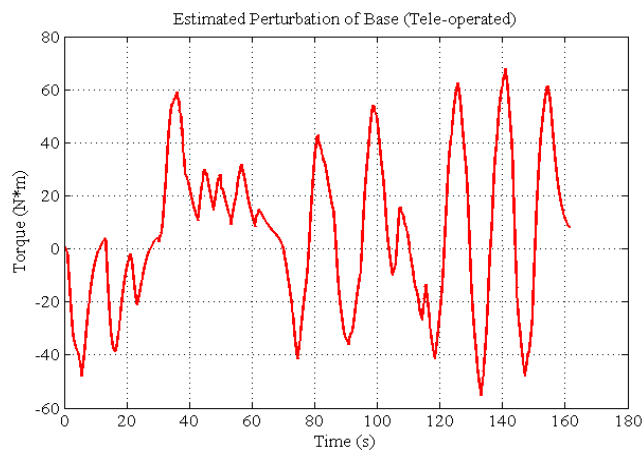


Figure 22. Estimated perturbation of the base for the master.

Figure 23 presents the experimental results for the end effector and the second link achieved using SMCSPO. At the start, for the first 4.1 s, the end effector and the 2nd link could not move. After 4.1 s, only the end effector was able to move until 13.5 s. Again, the end effector and the 2nd link could not move for another 0.7 s (i.e., from 13.5 to 14.2 s). Then, the 2nd link moved separately for 1.3 s (i.e., from 14.2 to 15.5 s). After that, the end effector and the 2nd link moved simultaneously for 6.5 s (i.e., from 15.5 to 22 s). Finally, the end effector and the 2nd link could not move for 7.1 s (i.e., from 22 to 29.1 s). The slave device followed the trajectory of the master device accurately. The maximum trajectories of the end effector and the 2nd link were 82.97 and 42.04 degrees, respectively.

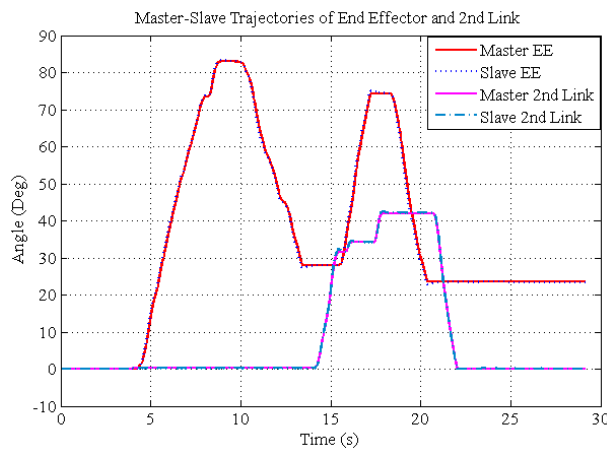


Figure 23. Master/slave trajectories for the end effector and the 2nd link.

7. Conclusions

This paper presented a methodology for estimating the reaction force for the base, 2nd link, and end effector of a 3DOF master and slave manipulator system. The advantageous feature of the proposed methodology is that it does not utilize any force sensors. In general, SMCSPO is implemented, whereby SMC-based tele-operated bilateral control and visual feedback generate the trajectory for the slave system with a minimum of tracking error. In addition, the tele-operated bilateral control strategy also estimates the reaction force of the master manipulator, which is used by the operator to control the master device.

The experimental results presented in this study indicate that the slave manipulator successfully tracked the master device with negligible error. It was also observed based on the results that the operator was able to feel the reaction force as the slave device touched/interacted with the environment, without the use of any feedback from force sensors. The maximum trajectories, error and perturbation between the master and the slave for the end effector, 2nd link and base are summarized in Table 4.

Table 4. Maximum trajectories, error and perturbation between master and slave.

S. No	Links	Maximum Error (Degree)	Maximum Trajectory (Degree)	Maximum Perturbation of Master (N*m)	Maximum Perturbation of Slave (N*m)
1	End Effector	0.94	88.96	90.87	1635.72
2	2 nd link	0.55	60.13	45.69	543.9
3	Base	0.859	100.38	67.89	1018.26

In the future, issues like latency and jitter in the global area network (GAN) should be addressed in order to enhance the tele-operation range. The area of application for this study was the dismantling of nuclear power plants, but the proposed method is not limited to this, as several other applications require master/slave systems in which human access is limited. These applications include hazardous areas

with high levels of radiation from materials with long half-lives. Examples of this include transportation of uranium in its active form, the disposal of explosive material, handling of explosive/radioactive material, remote cutting for nuclear plant dismantling, etc.

Author Contributions: Conceptualization, K.D.K. and M.C.L.; Formal analysis, K.D.K. and H.K.; Funding acquisition, M.C.L.; Investigation, J.W.; Methodology, K.D.K. and S.J.A.; Project administration, M.C.L.; Software, K.D.K.; Supervision, M.C.L.; Validation, S.J.A.; Writing—original draft, K.D.K. and J.W.; Writing—review & editing, H.K. and M.C.L.

Funding: This research was funded and conducted under “the Competency Development Program for Industry Specialists” of the Korean Ministry of Trade, Industry and Energy (MOTIE), operated by Korea Institute for Advancement of Technology (KIAT). (No. P0008473, the development of high skilled and innovative manpower to lead the Innovation based on Robot). This research was supported by the Technology Innovation Program (10073147, Development of Robot Manipulation Technology by Using Artificial Intelligence) funded By the Ministry of Trade, Industry & Energy (MOTIE, Korea).

Conflicts of Interest: The authors declare no conflicts of interest.

References

1. Available online: <https://www.iaea.org/pris/worldstatistics/operationalreactorsbycountry.aspx> (accessed on 15 August 2012).
2. Korean Prime Minister’s Office. *Development of 21 Core Technologies for Dismantling Nuclear Facilities until 2021*; Korean Prime Minister’s Office Press: Seoul, Korea, 2012.
3. Kim, K.; Jang, J. Domestic market prospect and core technology for decommissioning of nuclear power plant. *Korean Inst. Constr. Eng. Manag. Conf. J.* **2013**, *7*, 37–40.
4. Yasuhiko, M.; Mitsugu, T.; Hisashi, N.; Mitsuo, T.; Mutsuo, H.; Michiro, Y.; Satoshi, Y.; Kazuo, F. Results and outline of JPDR dismantling demonstration project. *Nippon Genshiryoku Gakkai Shi* **1996**, *38*, 553–576.
5. Fisher, J.J. *Applying Robots in Nuclear Applications*; Society of Manufacturing Engineers: Dearborn, MI, USA, 1985.
6. Clement, G.; Vertut, J.; Cregut, A.; Antione, P.; Guittet, J. Remote handling and transfer techniques in dismantling strategy. In Proceedings of the Seminar on Remote Handling in Nuclear Facilities, Oxford, UK, 2–5 October 1984; pp. 556–569.
7. Ma, S.; Hirose, S.; Yoshinada, H. Development of a hyper-redundant multijoint manipulator for maintenance of nuclear reactors. *Adv. Robot.* **1994**, *9*, 281–300.
8. Denmeade, T. A pioneer’s journey into the sarcophagus. *Nucl. Eng. Int.* **1998**, *43*, 18–20.
9. Varley, J. Windscale: Getting down to the core. *Nucl. Eng. Int.* **1997**, *12*, 26–28.
10. Benest, T. Taking up arms for decommissioning. *Nucl. Eng. Int.* **2004**, *49*, 14–16.
11. Tachibana, M.; Shimada, T.; Yanagihara, S. Development of remote dismantling systems for decommissioning of nuclear facilities. In Proceedings of the WM’00 Conference, Tucson, AZ, USA, 27 February–2 March 2000.
12. Bakari, M.J.; Zied, K.M.; Seward, D.W. Development of a multi-arm mobile robot for nuclear decommissioning tasks. *Int. J. Adv. Robot. Syst.* **2007**, *4*, 51. [[CrossRef](#)]
13. Dubus, G.; David, O.; Measson, Y.; Friconneau, J.-P.; Palmer, J. Making hydraulic manipulators cleaner and safer: From oil to demineralized water hydraulics. In Proceedings of the 2008 IEEE/RSJ International Conference on Intelligent Robots and Systems (IROS 2008), Nice, France, 22–26 September 2008; pp. 430–437.
14. Chabal, C.; Proietti, R.; Mante, J.-f.; Idasiak, J.-m. Virtual reality technologies: A way to verify dismantling operations, first application case in a highly radioactive cell. In Proceedings of the Fourth International Conference on Advances in Computer-Human Interaction, Guadeloupe, France, 23–28 February 2011.
15. Raju, G.J.; Verghese, G.C.; Sheridan, T.B. Design issues in 2-port network models of bilateral remote manipulation, robotics and automation. In Proceedings of the 1989 IEEE International Conference on Robotics and Automation, Scottsdale, AZ, USA, 14–19 May 1989; pp. 1316–1321.
16. Hashtrudi-Zaad, K.; Salcudean, S.E. Transparency in time-delayed systems and the effect of local force feedback for transparent teleoperation. *IEEE Trans. Robot. Autom.* **2002**, *18*, 108–114. [[CrossRef](#)]
17. Lawrence, D.A. Stability and transparency in bilateral teleoperation. *IEEE Trans. Robot. Autom.* **1993**, *9*, 624–637. [[CrossRef](#)]

18. Yokokohji, Y.; Yoshikawa, T. Bilateral control of master-slave manipulators for ideal kinesthetic coupling-formulation and experiment. *IEEE Trans. Robot. Autom.* **1994**, *10*, 605–620. [[CrossRef](#)]
19. Hannaford, B. A design framework for teleoperators with kinesthetic feedback. *IEEE Trans. Robot. Autom.* **1989**, *5*, 426–434. [[CrossRef](#)]
20. Adams, R.J.; Hannaford, B. Stable haptic interaction with virtual environments. *IEEE Trans. Robot. Autom.* **1999**, *15*, 465–474. [[CrossRef](#)]
21. Farooq, U.; Gu, J.; El-Hawary, M.; Asad, M.U.; Abbas, G. Fuzzy model based bilateral control design of nonlinear tele-operation system using method of state convergence. *IEEE Access* **2016**, *4*, 4119–4135. [[CrossRef](#)]
22. Yang, Y.; Hua, C.; Li, J.; Guan, X. Finite-time output-feedback synchronization control for bilateral teleoperation system via neural networks. *Inf. Sci.* **2017**, *406*, 216–233. [[CrossRef](#)]
23. Su, X. Master–slave control for active suspension systems with hydraulic actuator dynamics. *IEEE Access* **2017**, *5*, 3612–3621. [[CrossRef](#)]
24. Kallu, K.D.; Jie, W.; Lee, M.C. Sensorless reaction force estimation of the end effector of a dual-arm robot manipulator using sliding mode control with a sliding perturbation observer. *Int. J. Control Autom. Syst.* **2018**, *16*, 1367–1378. [[CrossRef](#)]
25. Truong, D.Q.; Truong, B.N.M.; Trung, N.T.; Nahian, S.A.; Ahn, K.K. Force reflecting joystick control for applications to bilateral teleoperation in construction machinery. *Int. J. Precis. Eng. Manuf.* **2017**, *18*, 301–315. [[CrossRef](#)]
26. Peñaloza-Mejía, O.; Márquez-Martínez, L.A.; Alvarez-Gallegos, J.; Alvarez, J. Master-slave teleoperation of underactuated mechanical systems with communication delays. *Int. J. Control Autom. Syst.* **2017**, *15*, 827–836. [[CrossRef](#)]
27. Mellah, R.; Guermah, S.; Toumi, R. Adaptive control of bilateral teleoperation system with compensatory neural-fuzzy controllers. *Int. J. Control Autom. Syst.* **2017**, *15*, 1949–1959. [[CrossRef](#)]
28. Xu, X.; Cizmeci, B.; Schuwerk, C.; Steinbach, E. Model-mediated teleoperation: Toward stable and transparent teleoperation systems. *IEEE Access* **2016**, *4*, 425–449. [[CrossRef](#)]
29. Liu, Y.-C.; Khong, M.-H.; Ou, T.-W. Nonlinear bilateral teleoperators with non-collocated remote controller over delayed network. *Mechatronics* **2017**, *45*, 25–36. [[CrossRef](#)]
30. Abut, T.; Soyguder, S. Real-time control of bilateral teleoperation system with adaptive computed torque method. *Ind. Robot Int. J.* **2017**, *44*, 299–311. [[CrossRef](#)]
31. Islam, S. State and impedance reflection based control interface for bilateral telerobotic system with asymmetric delay. *J. Intell. Robot. Syst.* **2017**, *87*, 425–438. [[CrossRef](#)]
32. Sun, D.; Naghdy, F.; Du, H. Time domain passivity control of time-delayed bilateral telerobotics with prescribed performance. *Nonlinear Dyn.* **2017**, *87*, 1253–1270. [[CrossRef](#)]
33. Azimifar, F.; Abrishamkar, M.; Farzaneh, B.; Sarhan, A.A.D.; Amini, H. Improving teleoperation system performance in the presence of estimated external force. *Robot. Comput. Integr. Manuf.* **2017**, *46*, 86–93. [[CrossRef](#)]
34. Sakaino, S.; Furuya, T.; Tsuji, T. Bilateral control between electric and hydraulic actuators using linearization of hydraulic actuators. *IEEE Trans. Ind. Electron.* **2017**, *64*, 4631–4641. [[CrossRef](#)]
35. Soltani, M.K.; Khanmohammadi, S.; Ghalichi, F.; Janabi-Sharifi, F. A soft robotics nonlinear hybrid position/force control for tendon driven catheters. *Int. J. Control Autom. Syst.* **2017**, *15*, 54–63. [[CrossRef](#)]
36. Wang, Y.; Jiang, S.; Chen, B.; Wu, H. Trajectory tracking control of underwater vehicle-manipulator system using discrete time delay estimation. *IEEE Access* **2017**, *5*, 7435–7443. [[CrossRef](#)]
37. Liu, X.; Jiang, W.; Dong, X.-C. Nonlinear adaptive control for dynamic and dead-zone uncertainties in robotic systems. *Int. J. Control Autom. Syst.* **2017**, *15*, 875–882. [[CrossRef](#)]
38. Li, Y.F.; Chen, X.B. On the dynamic behavior of a force/torque sensor for robots. *IEEE Trans. Instrum. Meas.* **1998**, *47*, 304–308. [[CrossRef](#)]
39. Cha, K.-G.; Yoon, S.-M.; Kim, H.-H.; Gim, K.-Y.; Lee, M.-C. Reaction force estimation of hydraulic servo system using sliding perturbation observer. In Proceedings of the 2015 IEEE International Conference on Advanced Intelligent Mechatronics (AIM), Busan, Korea, 7–11 July 2015; pp. 1754–1759.
40. Moura, J.T.; Elmali, H.; Olgac, N. Sliding mode control with sliding perturbation observer. *J. Dyn. Syst. Meas. Control* **1997**, *119*, 657–665. [[CrossRef](#)]

41. Moura, J.T.; Roy, R.G.; Olgac, N. Sliding mode control with perturbation estimation (smcpe) and frequency shaped sliding surfaces. *J. Dyn. Syst. Meas. Control* **1997**, *119*, 584–588. [[CrossRef](#)]
42. Slotine, J.-J.E.; Li, W. *Applied Nonlinear Control*; Prentice Hall: Englewood Cliffs, NJ, USA, 1991; Volume 199.
43. Cho, T.D.; Seo, S.H.; Yang, S.M. A study on the robust position control of single-rod hydraulic system. *J. Korean Soc. Precis. Eng.* **1999**, *16*, 128–135.
44. Mohieddine, J.; Kroll, A. *Hydraulic Servo-System: Modelling Identification and Control*; Springer Science & Business Media: New York, NY, USA, 2012.
45. Lee, M.C.; Aoshima, N. Identification and its evaluation of the system with a nonlinear element by signal compression method. *Trans. Soc. Instrum. Control* **1989**, *25*, 729–736.



© 2019 by the authors. Licensee MDPI, Basel, Switzerland. This article is an open access article distributed under the terms and conditions of the Creative Commons Attribution (CC BY) license (<http://creativecommons.org/licenses/by/4.0/>).